Electrodeposition of tin oxide thin film from nitric acid solution: the role of pH

K. Daideche & A. Azizi

Journal of Materials Science: Materials in Electronics

ISSN 0957-4522
Volume 28
Number 11

J Mater Sci: Mater Electron (2017)
28:8051-8060
DOI 10.1007/s10854-017-6511-8

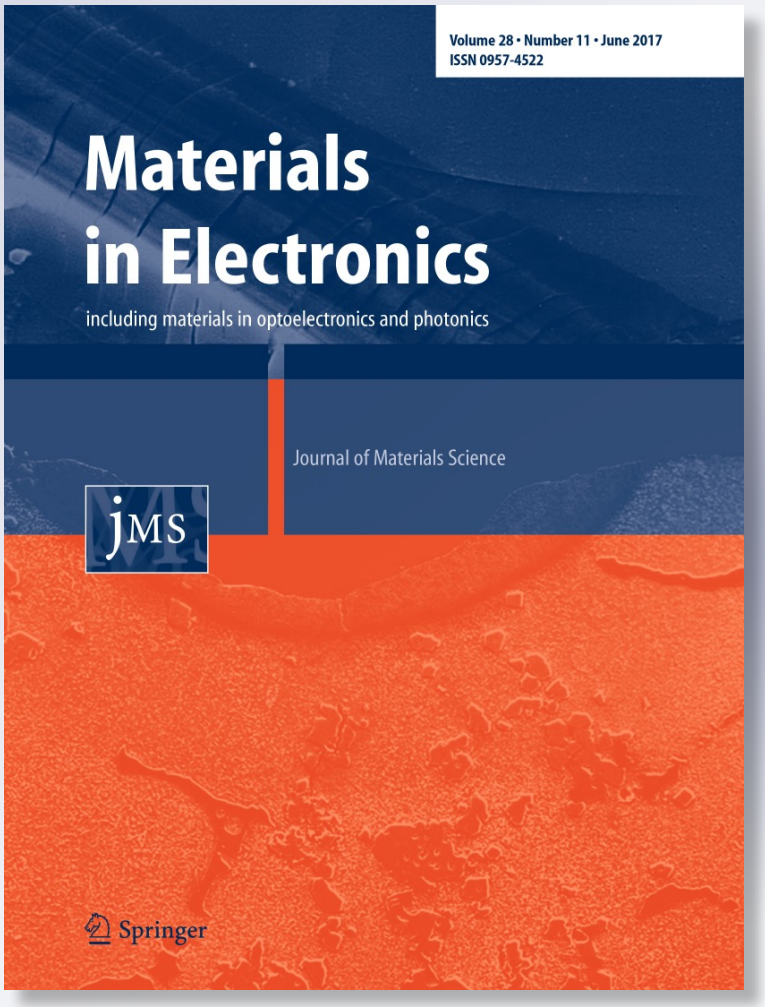

Springer

J Mater Sci: Mater Electron (2017) 28:8051–8060
DOI 10.1007/s10854-017-6511-8

Electrodeposition of tin oxide thin film from nitric acid solution: the role of pH

K. Daideche[1,2] · A. Azizi[1]

Received: 26 November 2016 / Accepted: 30 January 2017 / Published online: 17 February 2017

Abstract Tin oxide (SnO_2) thin films were synthesized by electrodeposition method from nitric acid medium with $SnCl_2$ precursor and $NaNO_3$ supporting electrolyte at 70 °C. The effect of pH electrolyte in the properties of SnO_2 thin films was investigated. Cyclic voltammetry (CV) was utilized for the determination of the selective potential for electrodeposition of pure SnO_2. Mott–Schottky (M–S) plots and electrochemical impedance spectroscopy (EIS) techniques were carried out to estimate the electrical characteristics of the SnO_2 thin films deposited at different pH electrolytes. These latter techniques show n-type conductivity for all the samples with optimal carrier density of $8.41 \times 10^{20}/cm^3$ and high value of conductivity for the films electrodeposited at pH ~ 1.10. Atomic force microscopy (AFM) observations showed that the SnO_2 thin films obtained at different pH are more homogenous in appearance and present lower surface roughnesses at lower pH value. Structural analysis of the SnO_2 thin films was performed by X-ray diffraction (XRD) which exhibit a polycrystalline structure for pH ~ 1.25 and amorphous one for another pH values. From the optical study, the transmittance and the gap energy were founded to be depending to the pH of electrolyte.

✉ A. Azizi
aziziamor@yahoo.fr; amorazizi@univ-setif.dz

[1] Laboratoire de Chimie, Ingénierie Moléculaire et Nanostructures, Université Ferhat Abbas-Sétif 1, 19000 Sétif, Algeria

[2] Centre de Recherche Scientifique et Technique en Analyses Physico-Chimiques, BP 384, Zone Industrielle Bou-Ismail RP, 42004 Tipaza, Algeria

1 Introduction

Tin oxide (SnO_2) is one of the interesting oxide semiconductors, which have attracted a considerable attention of many scientists and researchers due to their excellent properties. It is a transparent, n-type oxide and wide band gap (3.6 eV) semiconductor [1]. It has chemical stability, good electrical conductivity and high transmittance in visible light [2–4]. These properties are exploited in solar cells, as catalytic support materials, as solid-state chemical sensors and as high-capacity lithium-storage [5–9].

Many methods such as RF magnetron sputtering, pulsed-laser deposition (PLD), the sol–gel process, spray pyrolysis, hydrothermal method and electrochemical deposition, have been used to prepare SnO_2 nanostructures [10–15]. This latterwas very investigated due to its advantages like simplicity, low cost, low temperature process, deposition on large and complex areas and capability to controlling properties and morphology by different electrochemical parameters [16]. Different mechanisms and ways of electrodeposition were studied, for example, Wang et al. [7] have prepared the SnO_2 films with two-step process: electrodeposition of metallic Sn from aqueous solution of $SnCl_2$ followed by thermal oxidation at 600 °C for 8h to obtained tin oxide. Also, pulse potential technique under low potential of −0.6 V and high potential of −0.1 V versus Ag/AgCl was performed to remove the metallic Sn co-deposited with SnO_2 [17]. Chang et al. [18] in order to electrodeposit the tin oxide and to control the morphology by applied current densities realized a galvonostatic mode of electrodeposition. Li et al. [19] have prepared tin oxide by electrodeposition with various post treatments of the deposits, light irradiation, HNO_3^- water vapor treatment and sintering at 550 °C in order to improve the SnO_2 characteristics. However, a simple cathodic deposition was used

to electrodeposit tin oxide or other oxides semiconductors. This method based on the generate of hydroxyl ions by the reduction of the oxygen precursor presented in the electrolyte bath, the deposition of oxide was considered to involve hydroxide formation from the combination of hydroxyl and metallic ions on the electrode area followed by decomposition into oxide and water [18]. Several oxygen precursors can be utilized such as hydrogen peroxide [20]. Seshadri et al. [21] have dissolved oxygen molecular gas in electrolyte as precursor to obtain the hydroxyl ions for electrodeposition of cadmium oxide. Its well demonstrates that the nitrates bath were largely utilized in electrodeposition of many oxides such as cerium, iron and tin oxide [22–24].

A recent study on electrochemical deposition of tin oxide have shown that the electrolyte conditions, like deposition time and applied potential have a significant effect on physical and chemical properties of this semiconductor [25–27]. The other authors concentrate on the role of doping element for amelioration and controlling of their properties especially electrical characteristics [13, 28].

In this work, we have chosen the electrochemical route with one-step cathodic deposition without any treatment or supplement process to prepare SnO_2 thin films. We have prepared the SnO_2 thin films on ITO transparent conductive glass substrate in nitric acid medium with different electrolyte bath acidity (pH), because in our knowledge the investigated of pH effect on tin oxide thin films properties has not been reported yet. The detailed study of the formation and mechanisms were treated and discussed. The electrical and optical properties of SnO_2 thin films were studied as function of the electrolyte pH to predict the use of the both of crystalline and amorphous SnO_2 as TCO in solar cells.

2 Experiments procedures

The electrodeposition of SnO_2 thin films was carried out potentiotatically from aqueous electrolytic solution consisting of 40 mM $SnCl_2$, 100 mM HNO_3 and 100 mM $NaNO_3$ as supporting salt. HNO_3 acid was added to adjusting pH for obtaining various pH solutions: 1.25, 1.10, 0.8, 0.5 and 0.3. The deposition temperature was fixed at 70 °C by thermostatic bath and the electrolytic solution was stirred for 30 min to give stabilized solution. The chronoamperometry technique was used to electodeposited SnO_2 thin films at −0.9 V for 10 min.The thickness of the films was estimated at 400 nm by chronocoulomety technique, using Faraday law to give the same electric charge. Classical three electrode system was used to the electrodeposition procedure with a saturated calomel electrode (SCE) as a reference electrode, a Pt wire as a counter electrode, and an Indium doped SnO_2 (ITO) coated transparent glass as working electrode. Prior to the deposition process, the ITO substrates were ultrasonically cleaned in methanol, acetone and distillate water for 10 min and etched in nitric acid 45% for 2 min to activate the surface of the electrode, which fixed at 1 cm^2 area. The SnO_2 thin films obtained were rinsed with distillate water to remove the chloride contaminant and dried in air at ambient conditions.

Morphological characterization was performed by atomic force microscopy (MFD-3D Classic Asylum Research). Phase identification and crystallographic structure determination were carried out using X-ray diffraction (XRD) on a PANalytical X'Pert Pro MPD instrument, with $CuK_{\alpha 1}$ incident radiation source ($\lambda = 1.54056$ Å) in a θ–2θ geometry. The optical properties of the SnO_2 thin films were measured with an UV–Vis–NIR spectrophotometer (Shimadzu UV-1800) in the range of 200–1100 nm.

3 Results and discussion

Figure 1a shows the cyclic voltammetry (CV) of Pt wire in 100 mM nitric acid without and with the presence of the precursor (HNO_3) and ($HNO_3 + SnCl_2$), respectively. In supporting electrolyte (HNO_3), we observed a cathodic intense peak with ($E_p = -0.65$ mV vs. SCE, $i_p = -6.27$ mA/cm^2) which might be attributed to the reduction of NO_3^- ions (Eq. 1). In supporting electrolyte with the presence of the precursor ($HNO_3 + SnCl_2$), the cathodic peak became more intense with ($E_p = -0.60$ mV vs. SCE, $i_p = -16.13$ mA/cm^2). This increase in current intensity is due to the presence of the second reduction with close potential value with that of nitrates reduction, without forgetting the hydrogen evolution reaction (HER) occurred in acidic aqueous medium. The second reaction corresponded to the reduction of Sn^{4+} present in the electrolyte to the metallic Sn (Eq. 2), its well established that the Sn^{4+} ions is could be obtained by easy oxidation of Sn^{2+} by dissolved oxygen in the solution [17], or by nitric acid [26]

$$NO_3^- + H_2O + 2e^- \rightarrow NO_2^- + 2OH^- \quad (1)$$

$$Sn^{4+} + 2e^- \rightarrow Sn \quad (2)$$

The hydroxyl anions (OH^-) obtained by reduction of NO_3^- were chemically reacted with Sn^{4+} present in the solution to formed the tin hydroxide, it was instable and easily dehydrated by elevated temperature (70 °C) which leads to the deposition of SnO_2 thin films on cathodic area by following reactions:

$$Sn^{4+} + 4\ OH^- \rightarrow Sn(OH)_4$$

$$Sn(OH)_4 \rightarrow SnO_2 + H_2O \quad (4)$$

In the reversal of sweep direction, no anodic peak was observed for voltammogram in supporting electrolyte

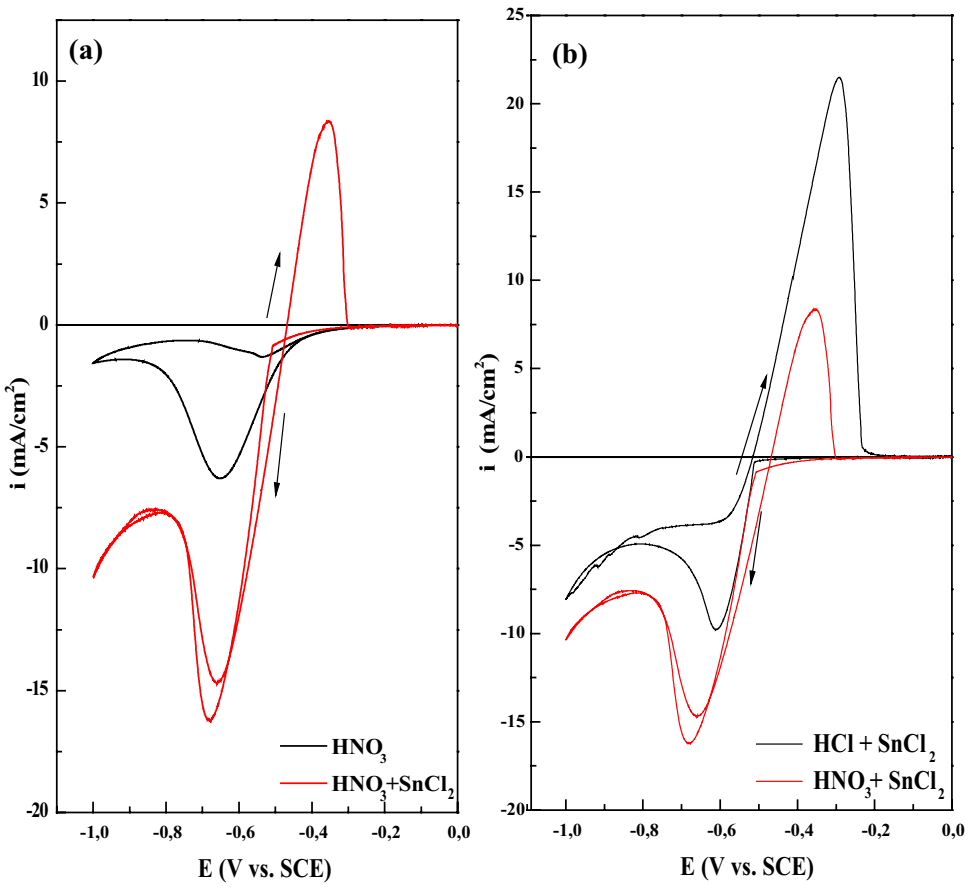

Fig. 1 Cyclic voltammograms of Pt wire at 50 mV/s: **a**100 mM nitric acid without and with the presence of 40 mM $SnCl_2$ and **b**100 mM nitric acid + 40 mM $SnCl_2$ and 100 mM chloridric acid + 40 mM $SnCl_2$

(HNO_3) which indicated that the reaction of nitrates reduction is irreversible. For the presence of $SnCl_2$ ($HNO_3 + SnCl_2$), a significant oxidation peak was observed during anodic sweep due to the oxidation of metallic Sn formed by the reduction of Sn^{4+}.

Figure 1b shows the cyclic voltammetry of Pt wire in nitric acid and hydrochloric acid with the presence of the precursor in both of electrolyte ($HCl + SnCl_2$) and ($HNO_3 + SnCl_2$) respectively. The same form of voltammogramwas observed but with lower cathodic peak in HCl electrolyte comparatively with that of HNO_3, this peak related to the reduction of Sn^{4+} only. In the reversal of sweep direction, an anodic peak was observed for two electrolytes, the oxidation peak intensity in HCl ($i_p = 21.41$ mA/cm^2) is the higher than that in HNO_3($i_p = 8.31$ mA/cm^2). From these results, we can say that the nitrates reduction is the predominant reaction and the essential one for tin oxide electrodeposition. Similar voltammograms had been also obtained by Chen et al. [17]. Our result is also very comparable with that of Anicia et al. [29] concerning potential values of cathodic tin deposition, which was in the range of −0.45 to −0.5 V, and with that of Baka et al. [30] for nitrate reduction with potential value of −0.7 V versus SCE. The electrochemical kinetic process of nitrates reduction was also investigated by CV technique at series of scan rates on Pt wire. Effectively, Fig. 2a shows the CV of Pt wire in 40 Mm $SnCl_2$ and 100 mM HNO_3 at various scan rates. It is clear that the current peak of nitrates reduction shows increasing with scan rate increasing with absence of oxidation peaks reflecting the irreversible system. The variation of current peak density with square root of scan rate was presented in Fig. 2b; this is not directly proportionally; it is a curve with concavity which was turned to the scan rate axis which indicated that the reduction of nitrate ions on Pt wire in this solution followed by chemical reaction. This result confirms the equations tired from cyclic voltammetry of Fig. 1, the OH^- formed during nitrate reduction reacted chemically with Sn^{4+} present in the solution to form the SnO_2 deposit.

The ideal comportment of semiconductor/electrolyte junction was described by Mott–Schottky (M–S) from depletion situation of semiconductor surface caused by achieved equilibrium condition in the interface semiconductor/electrolyte. It means equality in Fermi level of semiconductor with Fermi level of electrolyte, which corresponded to the E° (red/ox) present in the electrolyte. The variation of the capacitance of space charge region of SnO_2 thin films electrodeposited at various pH electrolyte versus

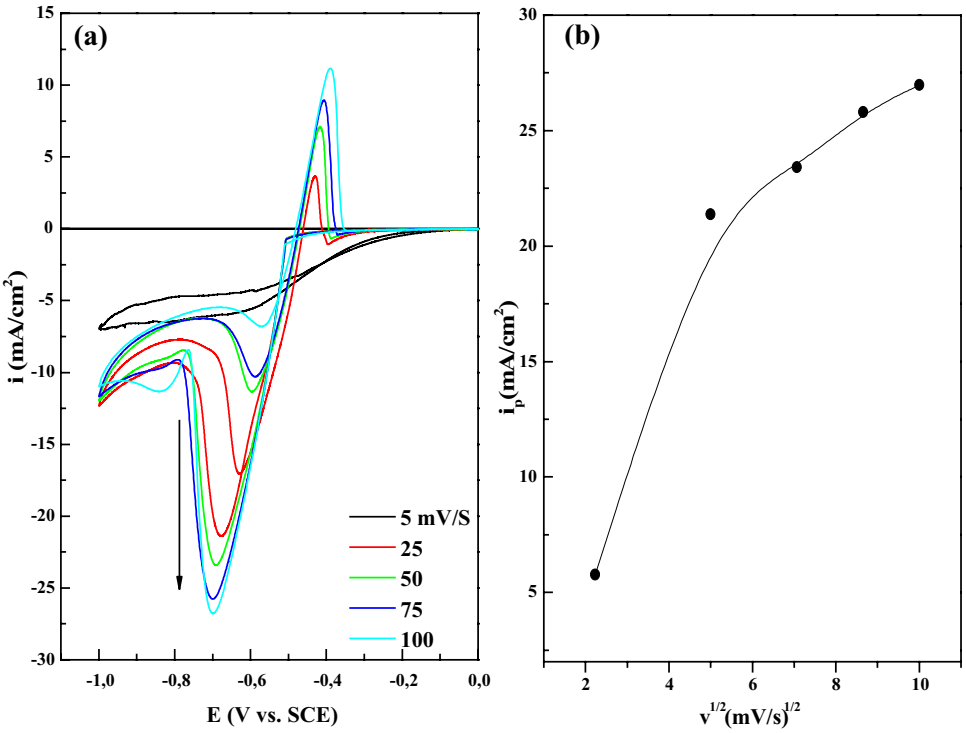

Fig. 2 **a** Cyclicvoltammogramms of Pt wire at various scan rate in 100 mMHNO$_3$ + 40 mM SnCl$_2$, and **b** Dependence of current peak to the square root of scan rate of nitrates reduction in 100 mM HNO_3^- + 40 mM SnCl$_2$

applied bias potential was carried out in 0.1 M NaNO$_3$ electrolyte with 500 Hz frequency following the Mott-Schottky relation for an n-type semiconductor [31]:

$$\frac{1}{C_{SC}^2} = \frac{2}{e\varepsilon\varepsilon 0 A^2 N_D}\left[V - V_{fb} - \frac{KT}{e}\right] \quad (5)$$

where ε_0 is the vacuum permittivity, ε is the relative permittivity of the semiconductor (ε of SnO$_2$ is 173[02]), e the elementary charge, ND the carrier concentration, Z the flat band potential, T the thermodynamic temperature and K is the Boltzmann's constant. The plots (Fig. 3) suggesting an n-type conductivity of all samples due to the positive slope of the linear curve [32]. In addition, this later gives the carrier concentration (N_D) of the samples and the extrapolating of the linear part of the M–S plots at $1/C_{sc}^2 = 0$ gives the V_{fb} of the samples. These useful parameters were presented in Table 1. The negative values of the flat band were in a good agreement with n type semiconductor and were positively shifted with decreasing pH from 1.10 to 0.3; the samples obtained at this pH of electrolyte were corresponded to the amorphous phases confirmed by XRD patterns (see Fig. 7). Liu et al. [33] have explained this effect by the low crystallinity of the samples. The carrier concentration was relatively high for different pH values; comparatively with SnO$_2$ doped indium of our substrate; the decreasing in the electrolyte pH has a greater effect on the increase of carriers density; the highest value of carrier concentration corresponded to pH ~ 0.8 and the lowest one corresponded to pH ~ 0.3. It was known that the oxygen

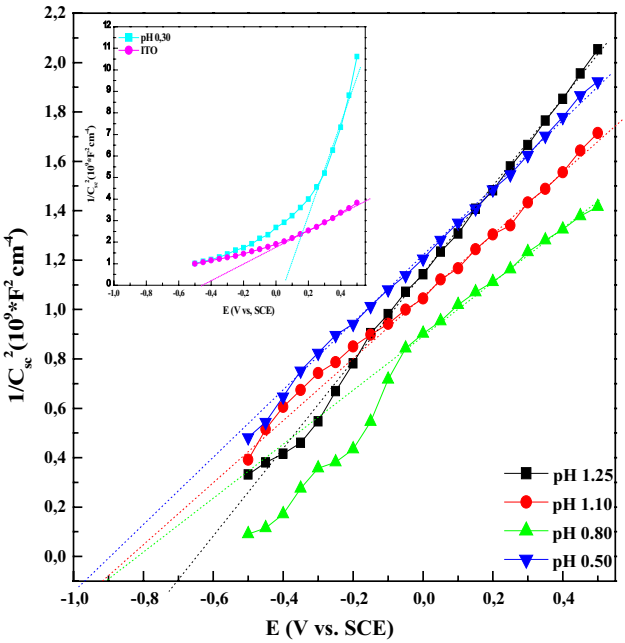

Fig. 3 Mott–Schottky plot of SnO$_2$ films electrodeposited at various electrolyte pH

vacancy or the interstitial cations are the source of n-type conduction in nonstochiometric intrinsic oxides and the oxygen vacancy is the predominant defect in tin oxide [34]. The increase of carrier's concentration with decreasing pH from pH ~ 1.25 (4.50×10^{20} cm^{-3}) to pH ~ 0.8 (8.41×10^{20}

Table 1 Variation of carrier's concentration and flat band of SnO_2 thin films versus electrolyte pH

pH	ITO	1.25	1.10	0.8	0.5	0.3
N_D (cm^{-3})	1.7×10^{20}	4.50×10^{20}	5.44×10^{20}	8.41×10^{20}	5.78×10^{20}	2.69×10^{13}
V_{fb} (V)	−0.289	−0.653	−0.955	−0.913	−0. 846	−0.147

cm^{-3}) can be attributed to the increase in creation of oxygen vacancy with tow electron liberated following Kroger-Vink notation (Eq. 6) [35]. The hydrogen molecules formed by co-reduction of H^+ during electrodeposition of the SnO_2 films were adsorbed in the surface of SnO_2 (Eq. 7 and 8) and may be reacted with oxygen gas which was liberated during the creation of oxygen vacancy leading to motivate the creation of this defects so more carrier's concentration. From the Mott–Schottky analysis we can predicted that the increasing of the conductivity of the SnO_2 films follows the sense of increasing of carrier concentration because of the proportionality existed among them. Our analysis is in agreement with Paria et al. [36], which were found that the electrical conductivity increases by increasing of defect concentration and the oxygen vacancy is the predominant defect in tin oxide. For the samples obtained at pH ~ 0.5 and 0.3, we are observed the decrease in carriers concentration with 5.78×10^{20} and 2.69×10^{13} cm^{-3} values, respectively. This regress in the carriers concentration for pH ~ 0.5 and especially for pH ~ 0.3 may be due to the decrease in oxygen vacancy caused by the decrease of the amount of the SnO_2 electrodeposited at these low pH values. This decrease of the growth of the SnO_2 thin films is observed in 3D AFM images (Fig. 5), which can be related to the increase of hydrogen evolution, as secondary concurrent reaction, with increasing the proton concentration by decreasing the electrolyte pH.

$$O_o \rightarrow \frac{1}{2}O_2 + Vo'' + 2e \qquad \text{Kroger - Vink notation} \qquad (6)$$

$$H^+ + 2e^- \rightarrow H_2 \qquad \text{Reduction} \qquad (7)$$

$$H_2(gas) = 2H\,(ads) \qquad \text{Adsorption} \qquad (8)$$

$$2H\,(ad) + \frac{1}{2}O_2 \rightarrow H_2O \qquad (9)$$

The electrochemical impedance spectroscopy (EIS) response of SnO_2 electrodeposited on ITO substrates at various pH solutions was carried out in 0.1 M $NaNO_3$ aqueous electrolyte in the range frequency of 0.01 Hz to 100 kHz with applied potential of −0.8 V versus SCE. Figure 4 shows the Nyquist diagrams of the samples, a semi circles were observed at high frequency, which corresponded to charge transfer in the interface electrode/electrolyte and the straight lines in the low frequency, which related to the diffusion of electro active spices [37]. The diameter of the

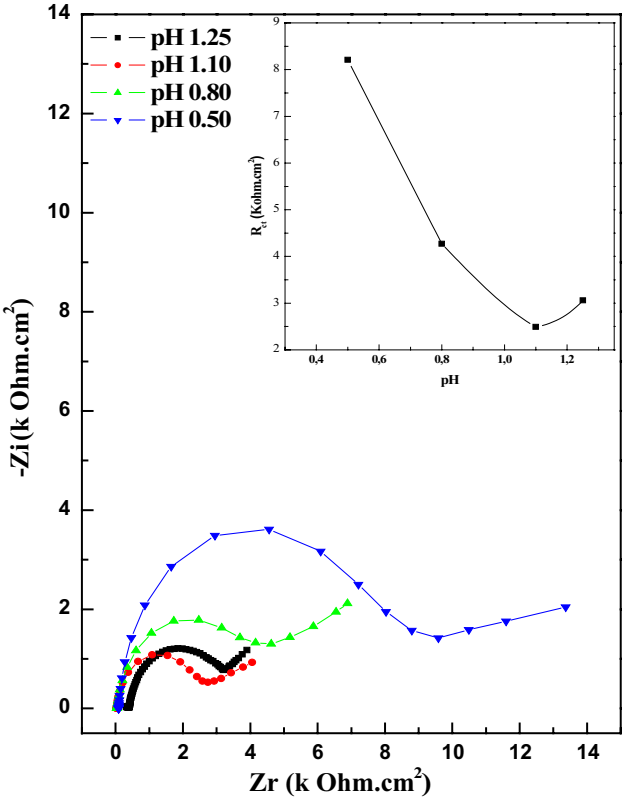

Fig. 4 Nyquist diagrams of ITO/SnO_2 films electrodeposited at various electrolyte pH in 0.1 M $NaNO_3$ aqueous electrolyte. The *inset* shows the corresponding variation of charge transfer resistance of the interfaces ITO/SnO_2/$NaNO_3$ with electrolyte pH

semicircle of ITO/SnO_2/$NaNO_3$ interface decreases from the films electrodeposited at pH ~ 0.5 to 0.8 to 1.25 and to pH ~ 1.10, which corresponded to the smaller semicircle suggesting that the film obtained at pH ~ 1.10 have a smaller charge transfer resistance (Rct); so the highest conductivity of this films. Despite the carrier concentration, value of the SnO_2 films obtained at pH ~ 0.8 and 0.5 was higher than that of the SnO_2 films obtained at pH ~ 1.10. The conductivity of the latter was the highest; we can explain this observation or contradiction by the presence of trapping states when we go to the amorphous and disordered phase of the SnO_2 electrodeposited at low pH values. For SnO_2 films electrodeposited at pH ~ 0.3, the EIS response was unclear and the points of diagram was randomly distributed which can be explained by the lower conductivity of the films which was confirmed by Mott–Schottky analyses, with a carrier concentration in order of 10^{13} cm^{-3}. The

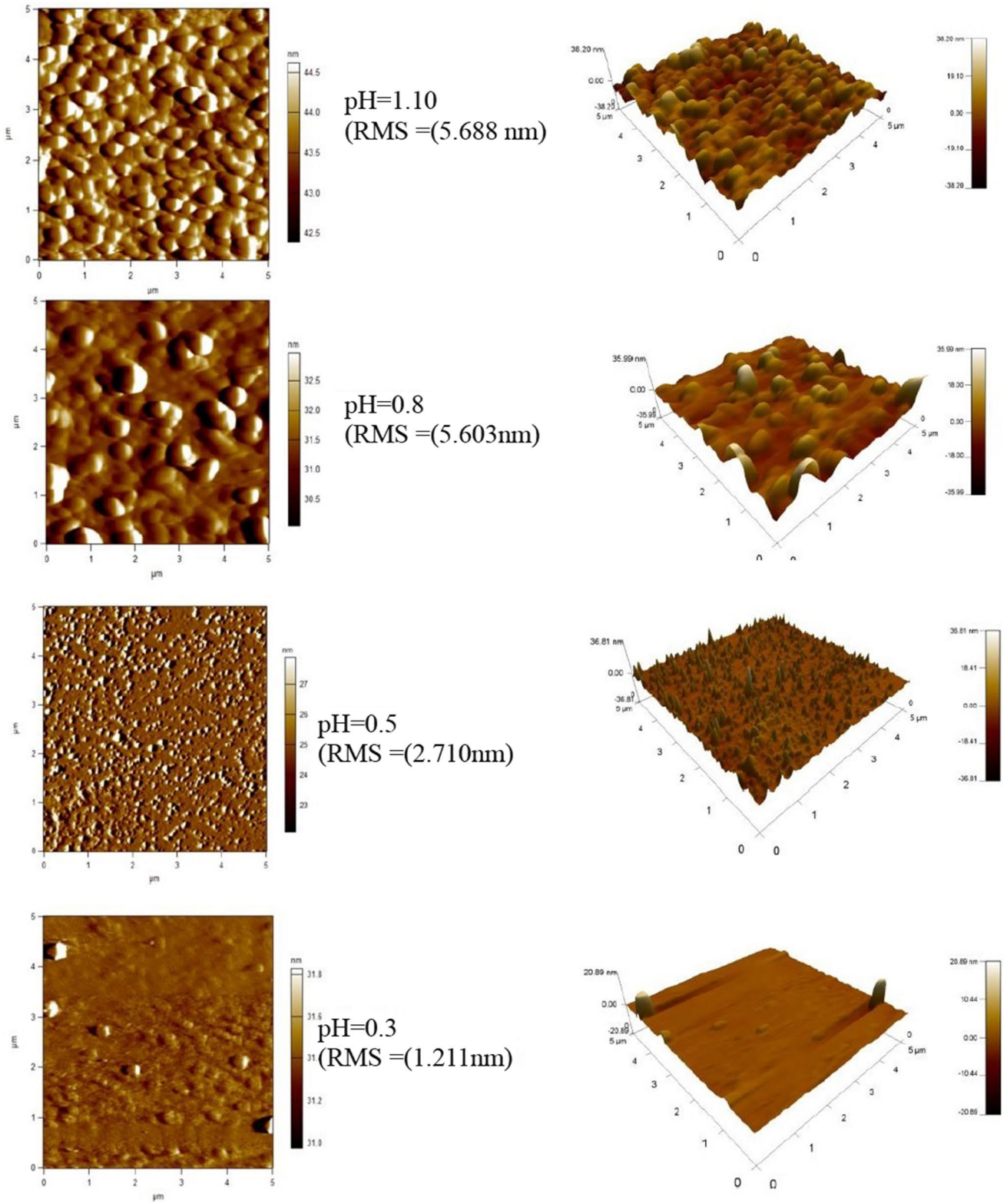

Fig. 5 2D and 3D AFM images of SnO_2 thin films electrodeposited on ITO substrate at various electrolyte pH

inset of Fig. 4 shows the corresponding variation of charge transfer resistance of the interfaces ITO/SnO_2/$NaNO_3$ with electrolyte pH.

The surface morphologies of the SnO_2 thin films grown on ITO substrates at various electrolytes pH were observed through atomic force microscopy (AFM). Figure 5 shows 2D and 3D AFM images with root mean square roughness (RMS) values correspondent of the deposits obtained by chronoamperometry at −0.9 V during 10 min. It is clear from 2D images that the electrolyte pH affects the films topography, where the grains size of the deposits was decreased with decreasing pH, which is in agreement with XRD results. In addition, we can have observed in 3D images the reduction of the deposit amount with deceasing pH, this was expected because of accompany of hydrogen evolution with the electrochemical formation of SnO_2 deposit which was evolved with decreasing pH. The root mean square roughness values decreased too with decreasing pH flow the order of grains size reduction. Karpuz et al. [38] observed similar effect of pH electrolyte on the morphologies (grains size and roughness) of Co–Mn films electrodeposited at different electrolyte pH by AFM analysis.

From the results, drown in cyclic voltammetry four values of potential around the reduction peak of nitrate ions −0.6, −0.7, −0.8 and −0.9 V were probable as selective potential for cathodic deposition of pure SnO_2 thin films. The phase purity and crystalline structure of SnO_2 samples were characterized using XRD technique. Effectively, Fig. 6 shows the XRD patterns of SnO_2 electrodeposited by chronoamperometry at 10 min at these different applied potentials. It is clear, from this patterns the sample deposited at −0.9 V show clear, sharp, and strong diffraction peaks. All the peaks in these patterns could be indexed as the tetragonal SnO_2 according to JCPDS card (No. 41-1445). Additionally, no diffraction features that are characteristic of impurities such as unreacted Sn and other tin oxides phases were observed, indicating the purity of the SnO_2 polycrystalline. Significant differences are observed between the samples deposited at others different deposition potentials. For SnO_2 oxides deposited at −0.8, −0.7 and −0.6 V a small Sn peaks impurities are observed which were disparate at −0.9 V. For this raison we have chosen a −0.9 V potential for SnO_2 electrodeposition. Figure 7 shows the XRD patterns of SnO_2 thin films electrodeposited under −0.9 V at 10 min at different values of pH solution. It was observed that the patterns of ITO substrate show diffraction peaks at 2θ values of 21.51°, 30.62°, 35.30°, 50.93°, and 60.65° correspond respectively to diffraction peaks of (211), (222), (400), (440) and (622) plans of cubic InO_2 phase of ITO substrate [39]. For thin films obtained at pH ~ 1.25, these patterns show crystalline diffraction peaks at 26,11°, 33.54°, 51.80° and 65° correspond respectively to (110), (101), (211), and (112) plans of SnO_2

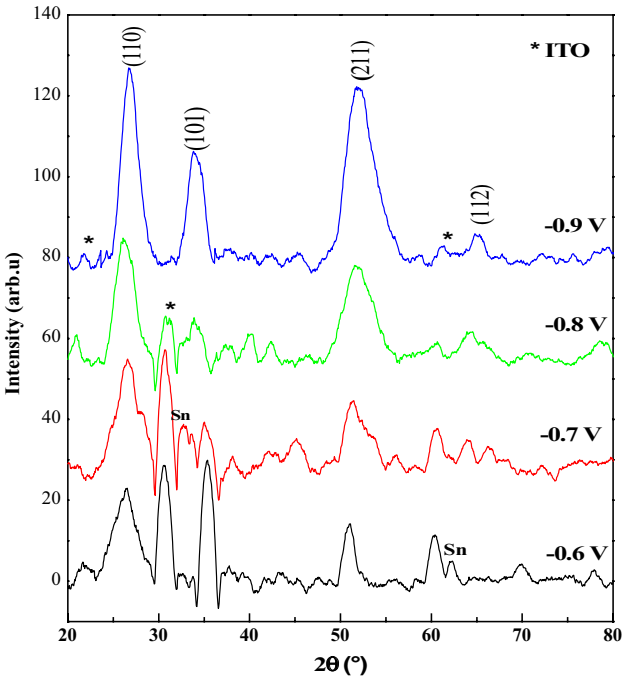

Fig. 6 XRD patterns of SnO_2 thin films electrodeposited at different applied potential

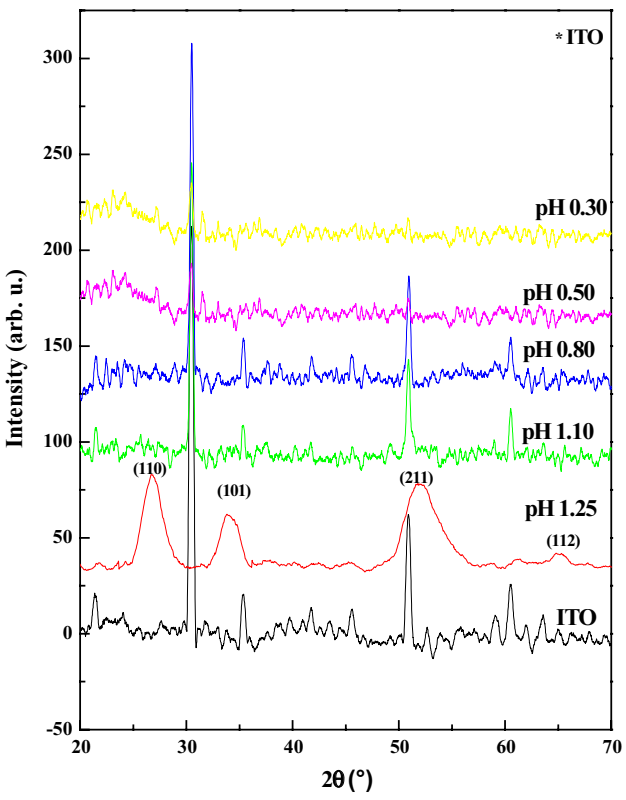

Fig. 7 XRD patterns of SnO_2 thin films obtained for 10 min deposition time at various electrolyte pH

crystal in accord with JCPDS (No. 41-1445). This is indicating the formation of SnO_2 thin films with tetragonal rutile structure at value of 1.25 pH electrolyte. The XRD patterns for the samples obtained at pH ~ 1.10 to 0.3 shows disappear of crystalline diffraction peaks and presence of only broad peak with decreasing pH, this is typical of an amorphous structure. In addition, the degree of amorphization may be increased in the sens of decreasing pH. We can explain this transition of SnO_2 crystalline structure (corresponded to pH ~ 1.25) to the SnO_2 amorphous phase (corresponded to another pH values) by the increase of the disorder with creation of defect (oxygen vacancy) which was motivated by decreasing the electrolyte pH i.e. increasing the H^+ concentration (Eqs. 6–9).

Valenzuela et al [39] obtained similar pattern of amorphous SnO_2 characteristics by broad peak, which have deposited the tin oxide by DC–magnetron sputtering, combined with thermal oxidation. Chang et al. [18] have explained in their work the presence of small broad peak in the patterns of electrodeposited SnO_2 by the low crystallinity and small particle size of the deposits, which mean the amorphous phase.

To study the influence of electrolyte pH on the optical properties of the grown SnO_2 thin films, transmittance measurements were conducted and the results are presented in Fig. 8. The dotted line which is parallel to X-axis is due to light transmittance of 80%. It was observed that all the samples exhibited high transmittance (>80%) in the visible region. A slight increase in transmittance from 82 to 83% for pH ~ 1.25 and 0.5, respectively; but noticeable increase in transmittance was observed for pH ~ 0.3, which attained 90%. The pH dependence of optical transmittance is related to the grain size and the surface roughnesse of the films. Its established that in the AFM analysis, the surface roughnesse were affected by the variation of electrolyte pH. This increase in transmittance with decreasing pH may be attributed to the decrease in light scattering resulting from reduction of surface roughness [40]; where the highest average optical transmittance of 90% corresponds to the lowest root mean square roughness value of 1.21 nm for pH ~ 0.3. The TCO semiconductors, polycrystalline or amorphous, suitable for use as thin films transparent electrode should have an average transmittance above 80% in visible range, carrier concentration of the order of 10^{20} cm^{-3} and gap energy above approximately 3 eV [41]. In this study, both of crystalline and amorphous SnO_2 thin films achieve these critters of TCO.

In order to determine the optical band gap of this material and the type of optical absorption, Tauc [42], Davis and Mott [43] showed that the absorption coefficient and photon energy are related by the following equation:

$$\alpha h\nu = A(h\nu - Eg)^n \tag{10}$$

In the above equation, A is a constant, Eg is the band gap of the material, α is the absorption coefficient, h the Plank constant, ν is the frequency of the radiation and n has different values depending on the optical absorption process. The corresponded optical band gap energies were estimated from the plot of $(\alpha h\nu)^2$ versus the photon energy (hν) (Fig. 9). The band gap was determined by the extrapolating

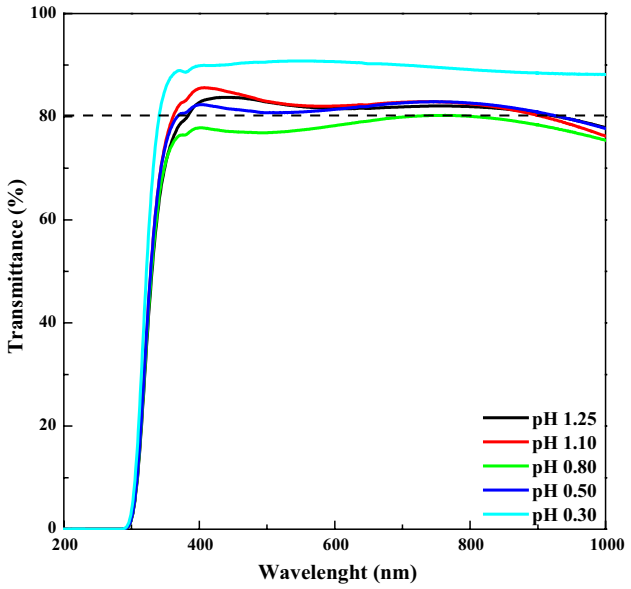

Fig. 8 Transmittance spectra of SnO_2 thin films electrodeposited at different electrolyte pH

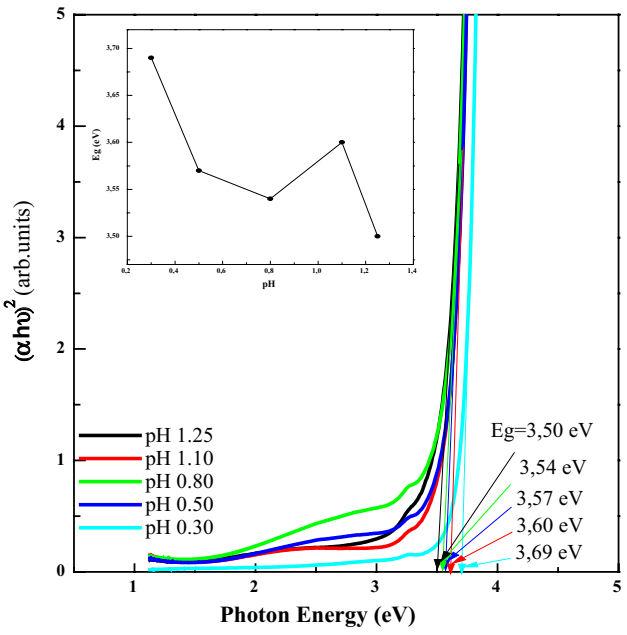

Fig. 9 Variation of $(\alpha h\nu)^2$ versus hν of SnO_2 thin films electrodeposited at different electrolyte pH. The inset shows the corresponding variation of the band gap of the samples with electrolyte pH

of the linear portion of the photon energy axis in the Tauc plot. The straight-line portion of the plots shown in Fig. 9 indicates the direct transition for all the samples [44]. The band gap values of the samples were confined between 3.50 and 3.69 eV; they were in good agreement with theoretical band gap value of 3.6 eV confirmed in literature. In the insert of Fig. 9 is presented the variation of the values of Eg with pH electrolyte. This curve indicates that the optical band gap increased generally with decreasing the pH of electrolyte; the pH dependence of the band gap is concerned with the crystallinity and the carriers concentration of the SnO_2 thin films. It was observed that for the samples obtained at pH ~ 1.25 corresponded to the polycrystalline films (well crystallinity); the band gap was taken the value of 3.50 eV is in a good agreement with that (3.52 eV) of undoped polycrystalline SnO_2 [45]. On the other hand, the band gap energies were increased with deceasing the pH, it was attained a maximum of 3.69 eV for pH ~ 0.3; in this range of pH, the SnO_2 films were amorphous phase with deteriorate crystallinity and reduction of the grain size. This effect is the quantum-size effect in semiconductors thin films [46]. In addition, the absorption edge shifts to the shorter wavelength with decreasing pH of electrolyte. Therefore, the SnO_2 thin films obtained with lower pH can absorb more UV light than the films electrodeposited at pH ~ 1.25. Also, the increase in values of band gap energy with decreasing electrolyte pH is due to the increase of carriers concentration (see the Mott–schottky analysis) with lowering pH, It's can be the Moss–Burstein effect [47].

4 Conclusion

The SnO_2 thin films were synthesized by electrochemical cathodic deposition under potential of −0.9 V versus SCE in nitric acid. The mechanism of the formation includes electrochemical reduction of nitrate ions to hydroxyl ions flowed by chemical step combined stannic and hydroxyl ions to formed tin oxide on electrode area. From the Mott–Schottky analysis and EIS measurements, it was founded that the electrical characteristics of the SnO_2 thin films were depended to the pH of the electrolyte and the critical value pH ~ 1.10, which corresponded to the higher conductivity with carrier's concentration in order of 5.44×10^{20} cm^{-3}. The morphology and the roughness of the deposits were significantly sensitive to change of the pH and were decreased with its decrease. It was revealed from XRD analysis that the cristallinity of SnO_2 films depend on the pH, which moves from polycrystalline to amorphous structure with decreasing pH. Optical transparency of the SnO_2 thin films was sufficient and increase in amorphous phase. Amorphous SnO_2 thin film combines between better electrical properties and adequate transparency for TCO application comparatively with crystalline SnO_2.

References

1. S.O. Kucheyev, T.F. Baumann, P.A. Sterne, Y.M. Wang, T. van Buuren, A.V. Hamza, L.J. Terminello, T.M. Willey, Phys. Rev.B 72, 035404 (2005).
2. A.E. Shalan, M. Rasly, I. Osama, M.M. Rashad, I.A. Ibrahim, J. Ceram. Int. **40**, 11619–11626 (2014)
3. S.T. Chang, I.C. Leu, M.H. Hon, J. Alloys Compd. 403, 335–340 (2005).
4. J. Yang, X. Li, S.L. Bai, R.X. Luo, A.F. Chen, Y. Lin, J.B. Zhang, J. Thin Solid Films **519**, 6241–6245 (2011)
5. J. Song, L. Hua, Q. Shen, F. Wang, L. Zhang, J. Key Eng. Mater. **633**, 273–276 (2015)
6. J. Long, W. Xue, X. Xie, Q. Gu, Y. Zhou, Y. Chi, W. Chen, Z. Ding, X. Wang, J. Catal. Commun. **16**, 215–219 (2011)
7. S. Wang, Y. Xiao, D. Shi, H.K. Liu, S.X. Dou, J. Mater. Chem. Phys. **130**, 1325–1328 (2011)
8. A. Sivashanmugam, T. Prem Kumar, N.G. Renganathan, S. Gopukumar, M. Wohlfahrt-Mehrens, J. Garche, J. Power Sources **144**, 197–203 (2005)
9. S. Das, V. Jayaraman. Prog. Mater. Sci. **66**, 112–255 (2014)
10. S. Yu, W. Yang, L. Li, W. Zhang, J. Sol. Energy Mater. Solar Cells 144, 652–656 (2016).
11. M. Okude, K. Ueno, S. Itoh, M. Kikuchi, A. Ohtomo, M. Kawasaki, J. Phys. D. **41**, 125309 (2008)
12. S. Sönmezoglu, A. Arslan, T. Serin, N. Serin, J. Phys. Scr. **84**, 065602 (2011)
13. M.M. Bagheri-Mohagheghi, M. Shokooh-Saremi, J. Phys. D. **37**, 1248–1253 (2004)
14. Y. Li, L. Qiao, L. Wang, Y. Zeng, W. Fu, H. Yang, Appl. Surf. Sci. **285**, 130–135 (2013)
15. S.T. Chang, I.C. Leu, M.H. Hon, J. Cryst. Growth. **273**, 195–202 (2004)
16. H. Ze-qianq, L. Xai-hai, X. Li-Zhi, M. Ming-you, W. Xian-ming, X. Zhuo-bing, L. Wen-ping, J. Cent. South. Univ. Technol. 12, 437–442(2005).
17. Z. Chen, Y. Tian, S. Li, H. Zheng, W. Zhang, J. Alloys Compd. **515**, 57–62 (2012)
18. S.T. Chang, I.C. Leuand, M.H. Hon, J. Electrochem. Solid-State Lett. **5**(8), C71–C74 (2002)
19. S. Li, Y. Li, Z. Chen, J. Liu, W. Zhang, J. Nanomater., 2012 Article ID 536810 (2012).
20. Th. Pauporte, D. Lincot, J. Electrochem. Soc. **148**(4), C310–C314 (2001)
21. A. Seshadri, N.R. de Tacconi, C.R. Chenthamarakshan, K. Rajeshwar. Electrochem. Solid-State Lett. **9**(1), C1–C4 (2006)
22. Y. Hamlaoui, F. Pedraza, C. Remazeilles, S. Cohendoz, C. Rebere, L. Tifouti, J. Creusa, J. Mater. Chem. Phys. **113**, 650–657 (2009)
23. T. Yousefi, R. Davarkhaha, A.N. Golikand, M.H. Mashhadizadeh, A. Abhari, J. Prog. Nat. Sci. **23**(1), 51–54 (2013)
24. M. Lai, J.H. Lim, S. Mubeen, Y. Rheem, A. Mulchandani, M. Deshusses, N.V. Myung, J. Nanotechnol. **20**, 185602 (2009)
25. S. Aydin, G. Turgut, M. Yilmaz, D. Tatar, B. Düzgün, M. Ertuğru, J. Phys. Sci. **7**(34), 5327–5333 (2012)
26. S. Kim, H. Lee, C.M. Park, Y. Jung, J. Nanosci. Nanotechnol. **12**, 1616–1619 (2012)
27. D. Lee, D.Y. Yun, Y.S. No, J.H. Hwang, C.H. Lee, T.W. Kim, J. Nanosci. Nanotechnol. **13**, 7596–7599 (2013)

28. H. Cheng, C. Wen, C. Hsu, J. Vac. Sci. Technol. A34, 01A112 (2016).
29. L. Anicai, A. Petica, S. Costovici, P. Prioteasa, T. Visan, J. Electrochim. Acta. **114**, 868–877 (2013)
30. O. Baka, A. Azizi, S. Velumani, G. Schmerber, A. Dinia, J. Mater. Sci-Mater. Electron. 25, 1761–1769 (2014)
31. F. Cardon, W.P. Gomest, J. Phys. D. **11**, L63–L67 (1978)
32. R. Xie, J. Su, M. Li, L. Guo, Int. J. Photoenergy ID **620134**, 7 (2013)
33. J. Liu, M. Shahid, Y. S. Ko, E. Kim, T.K. Ahn, J.H. Park, Y.U. Kwon, Phys. Chem. Chem. Phys., **15**, 9775 (2013).
34. M.K. Paria, H.S. Maiti, J. Mater. Sci. **17**, 3275–3280 (1982)
35. K.G. Godinho, A. Walsh, G.W. Watson, J. Phys. Chem. **C113**, 439–448 (2009)
36. M.K.P aria, H.S. Maiti, J. Mater. Sci. **18**, 2101–2107 (1983)
37. S. Abaci, B. Nessark, R. Boukherroub, K. Lmimouni, J. Thin Solid Films **519**, 3596–3602 (2011)
38. A. Karpuz, H. Kockar, M. Alper, Appl. Surf. Sci. **358**, 605–611 (2015)
39. J.J. Valenzuela-Jauregui, R. Quintero-Gonzalez, J. Hernandez-Torres, A. Mendoza-Galvan, R. Ramırez-Bon. J. Vac. **76**, 177–180 (2004)
40. A. Abhijit, Yadav. J. Thin Solid Films **591**, 18–24 (2015)
41. T. Minami, J. Semicond. Sci. Technol. **20**, S35–S44 (2005)
42. J. Tauc, In Optical properties of solids 22, ed. by F. Abeles (North Holland Publications, Amsterdam, 1970).
43. E. Burstein, Phys. Rev. **93**, 632 (1954)
44. H. Kim, C.M. Gilmore, A. Piqué, J.S. Horwitz, H. Mattoussi, J. Appl. Phys. **86**, 6451 (1999)
45. B. Xu, X.G. Ren, G.R. Gu, L.L. Lan, B.J. Wu, J. Superlattices Microstruct. 89, 34–42 (2016).
46. D. Bao, X. Yao, N. Wakiya, K. Shinozaki, N. Mizutani, J. Appl. Phys. Lett **79**, 3767 (2001)
47. H. Lahmar, A. Azizi, G. Schmerber, A. Dinia, RSC Adv. 6, 68663–68674 (2016)